The method of dynamic mode decomposition in shallow water and a swirling flow problem

Diana A. Bistrian[1,*,†] and Ionel M. Navon[2]

[1]*Department of Electrical Engineering and Industrial Informatics, Politehnica University of Timisoara, 331128 Hunedoara, Romania*
[2]*Department of Scientific Computing, Florida State University, Tallahassee, FL 32306-4120, USA*

SUMMARY

In this paper, a new vector-filtering criterion for dynamic modes selection is proposed that is able to extract dynamically relevant flow features from dynamic mode decomposition of time-resolved experimental or numerical data. We employ a novel modes selection criterion in parallel with the classic selection based on modes amplitudes, in order to analyze which of these procedures better highlight the coherent structures of the flow dynamics. Numerical tests are performed on two distinct problems. The efficiency of the proposed criterion is proved in retaining the most influential modes and reducing the size of the dynamic mode decomposition model. By applying the proposed filtering mode technique, the flow reconstruction error is shown to be significantly reduced. Copyright © 2016 John Wiley & Sons, Ltd.

1. INTRODUCTION

Among several snapshot-based model order reduction, proper orthogonal decomposition (POD) and dynamic mode decomposition (DMD) represent modal decomposition methods that are widely applied to study dynamics in different applications.

The well-known method of POD has been illustrated on a variety of examples ranging from fluid mechanics [1, 2], turbulent flows and oceanography [3–6], or engineering [7–9]. More recently, the POD approach has been incorporated for reduced order modeling purposes by Du *et al.* [10], Fang *et al.* [11], Stefanescu *et al.* [12], Dimitriu *et al.* [13], and Xiao *et al.* [14]. POD proved to be an effective technique also in inverse problems, as demonstrated by the work of Winton *et al.* [15], Chen *et al.* [16, 17], and Cao *et al.* [18, 19].

The method of DMD is rooted in the theory of Krylov subspaces [20–22] because of the original derivation of DMD as a variant of the Arnoldi algorithm [23] and was first introduced in 2008 by Schmid and Sesterhenn [24]. Only a year later, Rowley *et al.* [21] presented their theory of Koopman spectral analysis, which has its inception back in 1931 [25].

So far, we have noticed two directions in DMD technique, underlined in the two seminal papers on the topic, respectively [21, 22]. The straightforward approach is seeking a companion matrix employed to construct in a least-squares sense the final data vector as a linear combination of all previous data vectors [21, 26, 27]. Schmid [22] explored the similarities between POD and DMD and recommended a more well-conditioned algorithm for DMD.

---

*Correspondence to: Diana A. Bistrian, Department of Electrical Engineering and Industrial Informatics, Politehnica University of Timisoara, Revolutiei Str. Nr.5, 331128 Hunedoara, Romania.
†E-mail: diana.bistrian@fih.upt.ro

In DMD, the modes are not orthogonal, but one advantage of DMD compared with POD is that each DMD mode is associated with a pulsation, a growth rate, and each mode has a single distinct frequency. Owing to this feature, DMD method was originally used in nonlinear dynamics, for instance, by Muld et al. [28] and was just recently introduced in fluid mechanics [21, 29–31]. Mezic [32, 33] was the first to apply the DMD theory for the purposes of model reduction.

Recently, a novel data-driven modal decomposition of fluid flow is proposed by Noack et al. [34] comprising key features of POD and DMD. They introduced a recursive DMD technique considering modes that are orthogonal by construction. In contrast to DMD with exponentially growing or decaying oscillatory amplitudes, the novel recursive DMD identifies initial, maximum, and final fluctuation levels and was shown to be significantly better than DMD and POD.

The utility of DMD versus POD for model reduction is illustrated in our previous paper [35], in the study of shallow water problem. There are several major differences between these two decomposition methods. The spatial basis functions for DMD and POD respectively offer an insight of the coherent structures in the flow field. The differences between POD and DMD occur because of the principles of their respective decomposition methods. The time evolution of a DMD mode is influenced by the multiplication of the complex eigenvalue of the Koopman operator [25] weighted by the amplitude, while the time evolution of POD modes is described by the temporal coefficients. The POD modes are orthonormal in space with the energy inner product. In DMD, each mode oscillates at a single frequency, hence the expression that the DMD modes are orthogonal in time.

Selection of Koopman modes and amplitudes used for the flow reconstruction constitutes the source of many discussions among modal decomposition practitioners. For instance, Jovanovic et al. [36] introduced a low-rank DMD algorithm to identify an *a priori* specified number of modes that provide optimal approximation of experimental or numerical snapshots at a certain time interval. Consequently, the modes and frequencies that have strongest influence on the quality of approximation have been selected. Chen et al. [20] introduced an optimized DMD, which tailors the decomposition to a desired number of modes. This method minimizes the total residual over all data vectors and uses simulated annealing and quasi-Newton minimization iterative methods for selecting the frequencies.

In this work, a new criterion for dynamic modes selection is proposed that is able to extract dynamically relevant flow features from time-resolved experimental or numerical data. Our objective is to employ the improved modes selection in parallel with the classic selection based on modes amplitudes, in order to analyze which of these procedures better highlight the coherent structures of the flow dynamics.

The remainder of this paper is organized as follows. In Section 2, we recall the principles governing the DMD, and we provide the description of the DMD algorithm employed for decomposition of numerical data. In particular, we discuss the implementation of a novel criterion for optimal selection of the DMD modes as an alternative to the classic modes selection based on their amplitude. Sections 3 and 4 illustrate the impact of the aforementioned new criterion on the numerical results for the shallow water problem and a swirling flow problem, respectively. Summary and conclusions are drawn in the final section.

2. THE METHOD OF DYNAMIC MODE DECOMPOSITION

2.1. *The principles of dynamic mode decomposition*

The Koopman operator is rooted in the work of French-born American mathematician Bernard Osgood Koopman [25]. Considering a dynamical system evolving on a manifold $\mathbb{M}$ such that, for all $v_k \in \mathbb{M}$, $v_{k+1} = f(v_k)$, the Koopman operator maps any scalar-valued function $g : \mathbb{M} \to \mathbb{R}$ into a new function Vg given by the following:

$$Vg(v) = g(f(v)). \tag{1}$$

Most informative on the spectral properties of the Koopman linear operator are the papers authored by independent investigators such as Rowley et al. [21, 27], Chen et al. [20], and Bagheri [37], where a rigorous treatment on the subject is given.

Assuming that $\{v_0, v_1, \ldots, v_N\}$ is a data sequence collected at a constant sampling time Δt, the DMD algorithm is based on the hypothesis that a Koopman operator $\mathcal{A}$ exists, which steps forward in time the snapshots, such that the snapshots data set

$$\{v_0, \, \mathcal{A}v_0, \, \mathcal{A}^2 v_0, \ldots, \, \mathcal{A}^{N-1} v_0\} \tag{2}$$

corresponds to the Nth Krylov subspace generated by the Koopman operator from v_0. The goal of DMD is to determine eigenvalues and eigenvectors of the unknown matrix operator $\mathcal{A}$; thus, a Galerkin projection of $\mathcal{A}$ onto the subspace spanned by the snapshots is performed. For a sufficiently long sequence of the snapshots, we suppose that the last snapshot v_N can be written as a linear combination of previous $N-1$ vectors, such that

$$v_N = c_0 v_0 + c_1 v_1 + \cdots + c_{N-1} v_{N-1} + \mathcal{R}, \tag{3}$$

in which $c_i, i = 0, \ldots, N-1$ are complex numbers and $\mathcal{R}$ is the residual vector. We assemble the following relations:

$$\mathcal{A}\{v_0, v_1, \ldots, v_{N-1}\} = \{v_1, v_2, \ldots, v_N\} = \{v_1, v_2, \ldots, V_0^{N-1} c\} + \mathcal{R}e_{N-1}^T, \tag{4}$$

where $V_0^{N-1} = \left(v_0, \, v_1, \, \ldots, \, v_{N-1} \right), c^T = \left(c_0, \, c_1, \, \ldots, \, c_{N-1} \right)$ is the unknown complex column vector, and e_j^T represents the jth Euclidean unitary vector of length $N-1$.

In matrix notation form, Eq. (4) reads

$$\mathcal{A}V_0^{N-1} = V_0^{N-1}\mathcal{C} + \mathcal{R}e_{N-1}^T, \quad \mathcal{C} = \begin{pmatrix} 0 & \ldots & 0 & c_0 \\ 1 & & 0 & c_1 \\ \vdots & \vdots & \vdots & \vdots \\ 0 & \ldots & 1 & c_{N-1} \end{pmatrix}, \tag{5}$$

where $\mathcal{C}$ is the companion matrix.

A direct consequence of (5) is that decreasing the residual increases overall convergence and therefore the eigenvalues of the companion matrix $\mathcal{C}$ will converge toward some eigenvalues of the Koopman operator $\mathcal{A}$.

The quantitative capabilities of DMD have already been well demonstrated in the literature, and several DMD procedures have been released by the efforts of Rowley *et al.* [21], Schmid [22], Bagheri [37], Mezic [33], Belson *et al.* [38], and Williams *et al.* [39]. The representation of data in terms of DMD is given by the linear model:

$$y_{DMD}{}^t(x) = \sum_{j=1}^{m} a_j \phi_j(\mathbf{x}) \lambda_j^{t-1}, \quad \lambda_j = e^{(\sigma_j + i\omega_j)\Delta t}, \quad t = 1, \ldots, N, \tag{6}$$

where the right eigenvectors $\phi_j \in \mathbb{C}$ are dynamic (Koopman) modes, the eigenvalues λ_j are called Ritz values [40], and coefficients $a_j \in \mathbb{C}$ are denoted as amplitudes or Koopman eigenfunctions. Each Ritz value λ_j is associated with the growth rate $\sigma_j = \frac{\log(|\lambda_j|)}{\Delta t}$ and the frequency $\omega_j = \frac{\arg(|\lambda_j|)}{\Delta t}$ and m represents the number of DMD modes involved in reconstruction.

The DMD algorithm that we applied in the forthcoming section for two distinct problems in hydrodynamics is based on the procedure proposed by Rowley [21] and proceeds as follows:

(1) Collect data $y_i(t, \mathbf{x}) = y(t_i, \mathbf{x})$, $t_i = i\Delta t$, $i = 0, \ldots, N$, and $\mathbf{x}$ representing the spatial coordinates whether Cartesian or cylindrical and form the snapshot matrix $V = \left[y_0, \, y_1, \, \ldots, \, y_N \right]$.

(2) A matrix V_1^{N-1} is formed with the first N columns, and the matrix V_2^N contains the last N columns of V: $V_1^{N-1} = \left[y_0, \, y_1, \, \ldots, \, y_{N-1} \right], V_2^N = \left[y_1, \, y_2, \, \ldots, \, y_N \right]$.

(3) Express V_2^N as a linear combination of the independent sequence V_1^{N-1}: $V_2^N = AV_1^{N-1} = V_1^{N-1}S + R$, where R is the residual matrix and S approximates the eigenvalues of A when $\|R\|_2 \to 0$. The objective at this step is to solve the minimization problem:

$$\underset{S}{Minimize}\ R = \left\| V_2^N - V_1^{N-1} S \right\|_2.$$

(4) We identify the singular value decomposition of V_1^{N-1}: $V_1^{N-1} = U \Sigma W^H$, where U contains the proper orthogonal modes of V_1^{N-1}, Σ contains the singular values, and W^H is the conjugate transpose of W. The use of this approach allows avoiding the use of the QR-decomposition when the matrix V_0^{N-1} is rank deficient [22].

(5) This step aims to compute S, and for the reader information, we will detail it in the following. Relations $AV_1^{N-1} = V_2^N = V_1^{N-1} S + R, \quad \|R\|_2 \to 0$ and $V_1^{N-1} = U \Sigma W^H$ yield:

$$\begin{aligned} AU\Sigma W^H = V_2^N &= U\Sigma W^H S \\ \Rightarrow \quad U^H AU\Sigma W^H &= U^H U\Sigma W^H S \\ \Rightarrow \quad S &= U^H AU. \end{aligned}$$

From $AU\Sigma W^H = V_2^N$, it follows that $AU = V_2^N W\Sigma^{-1}$ and hence $S = U^H \left(V_2^N W\Sigma^{-1}\right)$.

(6) The procedure to compute dynamic modes consists in solving the eigenvalue problem $SX = X\Lambda$ and obtain the dynamic modes as $\Phi = UX$. The diagonal entries of Λ represent the eigenvalues λ.

(7) The vector containing dynamic modes amplitudes $Ampl = \left(a_j\right)_{j=1}^{rank(\Lambda)}$ is obtained projecting dynamic modes onto the first snapshot.

(8) As a result of the presented algorithm, the reconstructed flow involving the DMD modes is given by the product:

$$V_1^{DMD} = \Phi \cdot diag(Ampl) \cdot Van, \tag{7}$$

where the Vandermonde matrix is

$$Van = \begin{pmatrix} 1 & \lambda_1^1 & \lambda_1^2 & \dots & \lambda_1^{N-2} \\ 1 & \lambda_2^1 & \lambda_2^2 & \dots & \lambda_2^{N-2} \\ 1 & \vdots & \vdots & \vdots & \vdots \\ \dots & \dots & \dots & \dots & \dots \\ 1 & \lambda_m^1 & \lambda_m^2 & \dots & \lambda_m^{N-2} \end{pmatrix}.$$

2.2. Selection of dynamic modes

The modes' selection, which is central in model reduction, constitutes the source of many discussions among modal decomposition practitioners. A low-rank DMD algorithm to identify an *a priori* specified number of modes that provide optimal approximation of experimental or numerical snapshots was introduced by Jovanovic *et al.* [36]. An optimized DMD method was recently introduced by Chen *et al.* [20], which tailors the decomposition to a desired number of modes. Their technique minimizes the total residual over all data vectors and uses simulated annealing and quasi-Newton minimization methods for selecting the frequencies. Tissot *et al.* [41] propose a new energetic criterion for model reduction using DMD, which incorporates the growth rate of the modes.

The superposition of all Koopman modes, weighted by their amplitudes and complex frequencies, approximates the entire data sequence, but there are also modes that have a weak contribution.

Bistrian and Navon [35] aimed to present a preliminary survey on DMD modes selection. In this previous investigation, we introduced a novel selection method for the DMD modes, associated amplitudes, and Ritz values to derive a DMD reduced-order model of the shallow water equations. We arranged the Koopman modes in descending order of the energy of the DMD modes weighted by the inverse of the Strouhal number. We eliminated the modes that contribute weakly to the data sequence based on the conservation of quadratic integral invariants by the reduced order flow. We address in this section the problem of identification of a small subset of DMD modes that yield an optimal truncated representation of the flow field in order to capture its most important dynamic structures.

A criterion of selecting the DMD modes can be their amplitude a_j. Assuming that, for a particular problem investigated here, there are no modes that are very rapidly damped having very high amplitudes, we explore the selection of the modes based on sorting them in decreasing order of their amplitudes. We define the relative error as the L_2-norm of the difference between the variables of the full model and approximate DMD solutions over the exact one, that is,

$$Er_{DMD} = \frac{\|y(\mathbf{x}) - y_{DMD}(\mathbf{x})\|_2}{\|y(\mathbf{x})\|_2}, \tag{8}$$

where $y(\mathbf{x})$ represent the full solution of the model and $y_{DMD}(\mathbf{x})$ represent the DMD solution. We retain dynamic modes and associated frequencies in descending order of their amplitudes until a minimum relative error of reconstruction is achieved:

$$\arg\min_m \{a_1 > a_2 > \cdots > a_m, \ Er_{DMD} \leqslant \varepsilon\}, \quad \varepsilon = 10^{-4}. \tag{9}$$

The flow dynamics may be unpredictable and exhibit modes with very high amplitudes but which are very fast damped, or rapidly growing modes having lower amplitudes. Therefore, the selection of modes based on their amplitude is not efficient as reported also by Noack *et al.* [42]. A different option could be the modes selection based on their frequency ω_j. This is not rigorous because it relies on *a priori* physical knowledge of the flow. The frequencies resolved by the DMD are still subjected to the Nyquist sampling theorem [43], and it is better to know in advance frequencies that are essential in the flow physics to adjust the sampling interval Δt.

To overcome these difficulties, we introduce in the following a new vector-filtering criterion for which the amplitude of any mode is weighted by its growth rate. This new dynamic filtering criterion is perfectly adapted to the flow dynamics and selects the modes that are dominant in both situations described previously. We define the amplification of any mode j as follows:

$$A_j = \frac{1}{T}\int_0^T a_j\left(\lambda_j^{t/\Delta t} + \lambda_j^{-t/\Delta t}\right)dt = a_j\frac{e^{\sigma_j T} + e^{-\sigma_j T} - 2}{\sigma_j T}, \quad T = (N-1)\Delta t. \tag{10}$$

We retain dynamic modes and associated frequencies in descending order of their amplification defined by (10) until a minimum relative error of reconstruction is achieved:

$$\arg\min_m \{A_1 > A_2 > \cdots > A_m, \ Er_{DMD} \leqslant \varepsilon\}, \quad \varepsilon = 10^{-4}. \tag{11}$$

Consequently, the modes and frequencies that have strongest influence on the quality of approximation are selected to be included in the reduced order model. We devote the next sections to illustrate the numerical results obtained upon application of the two aforementioned selection criteria for distinct hydrodynamic problems.

3. NUMERICAL RESULTS FOR SHALLOW WATER PROBLEM

The shallow-water equations have been used for a wide variety of hydrological and geophysical fluid dynamics phenomena such as tide-currents [44], pollutant dispersion [45], storm surges, or tsunami wave propagation [46]. In the Cartesian coordinates formulation, we suppose there exists a time-dependent flow $w = (u, v, h)(x, y, t)$ and a given initial flow $w(x, y, 0) = (u_0, v_0, h_0)(x, y)$, which are solutions of the Saint Venant equations, also called the shallow-water equations [47]:

$$u_t + uu_x + vu_y + \eta_x - fv = 0, \tag{12}$$

$$v_t + uv_x + vv_y + \eta_y + fu = 0, \tag{13}$$

$$\eta_t + (\eta u)_x + (\eta v)_y = 0, \tag{14}$$

where $u(x, y, t)$ and $v(x, y, t)$ are the velocity components in the x and y axis, respectively, $\eta(x, y, t) = gh(x, y, t)$ is the geopotential height, $h(x, y, t)$ represents the depth of the fluid, f

is the Coriolis factor, and g is the acceleration of gravity. Subscripts represent the derivatives with respect to time and the streamwise and spanwise coordinates.

We consider that the reference computational configuration is the rectangular two-dimensional domain $\Omega = [0, L_{max}] \times [0, D_{max}]$. The model (12)–(14) is considered here in a β-plane assumption [48], in which the effect of the earth's sphericity is modeled by a linear variation in the Coriolis factor:

$$f = \widehat{f} + \frac{\beta}{2} (2y - D_{max}), \tag{15}$$

where $\widehat{f}$ and β are constants and L_{max} and D_{max} are the dimensions of the rectangular domain of integration Ω, associated with periodic boundary conditions in the x-direction and solid wall boundary condition in the y-direction:

$$w(0, y, t) = w(L_{max}, y, t), \ v(x, 0, t) = v(x, D_{max}, t) = 0. \tag{16}$$

The initial condition introduced by Grammeltvedt in section 6 of [49] was adopted as the initial height field, which has been tested by different researchers [50–53], that is,

$$h_0(x, y) = H_0 + H_1 \tanh\left(\frac{9(D_{max}/2 - y)}{2D_{max}}\right) + H_2 \sin\left(\frac{2\pi x}{L_{max}}\right) \cosh^{-2}\left(\frac{9(D_{max}/2 - y)}{D_{max}}\right), \tag{17}$$

which propagates the energy in wave number 1, in the streamwise direction. Using the geostrophic relationship, $u = -h_y (g/f)$, and $v = h_x (g/f)$, the initial velocity fields are derived as follows:

$$u_0(x, y) = -\frac{g}{f} \frac{9H_1}{2D_{max}} \left(\tanh^2\left(\frac{9D_{max}/2 - 9y}{2D_{max}}\right) - 1\right) -$$

$$\frac{18g}{f} H_2 \sinh\left(\frac{9D_{max}/2 - 9y}{D_{max}}\right) \frac{\sin\left(\frac{2\pi x}{L_{max}}\right)}{D_{max}\cosh^3\left(\frac{9D_{max}/2 - 9y}{D_{max}}\right)}, \tag{18}$$

$$v_0(x, y) = 2\pi H_2 \frac{g}{f L_{max}} \cos\left(\frac{2\pi x}{L_{max}}\right) \cosh^{-2}\left(\frac{9(D_{max}/2 - y)}{D_{max}}\right). \tag{19}$$

We have followed the approach used by Navon [48] to implement a two-stage finite-element Numerov–Galerkin method for integrating the nonlinear shallow-water equations on a β-plane limited-area domain. This method when applied to meteorological and oceanographic problems gives an accurate phase propagation and also handles nonlinearities well. The accuracy of temporal and spatial discretization scheme equals $\mathcal{O}\left(k^2, h^p\right)$, where p varies in the interval $[4, 8]$. Using the numerical integration scheme detailed in [48], we have captured the shallow-water dynamics over long-term numerical integrations (10–20 days). The dimensional constants used for the model are as follows:

$$\widehat{f} = 10^{-4} s^{-1}, \quad \beta = 1.5 \times 10^{-11} s^{-1} m^{-1}, \quad g = 10 \, m s^{-1},$$

$$D_{max} = 4400 \, km, \quad L_{max} = 6000 \, km, \quad H_0 = 2000 \, m, \quad H_1 = 220 \, m, \quad H_2 = 133 \, m. \tag{20}$$

The two-stage finite-element Numerov–Galerkin method for integrating the nonlinear shallow-water equations on a β-plane limited-area domain proposed by Navon [48] was employed in order to obtain the numerical solution of the shallow-water equations model (12)–(14) associated with the initial conditions (17)–(19). In Figure 1, the initial fields are presented.

As an alternative to different modes selection methods existing in the literature, we explore both the selection criteria (9) and (11) when DMD algorithm is applied to the shallow-water problem. We record a number of 240 unsteady solutions of the two-dimensional shallow water equations model (12)–(14), with time step $\Delta t = 600 s$. The solutions of geopotential height field h and streamwise–spanwise fields (u, v) at $T = 31h$ are illustrated in Figures 2 and 3, respectively.
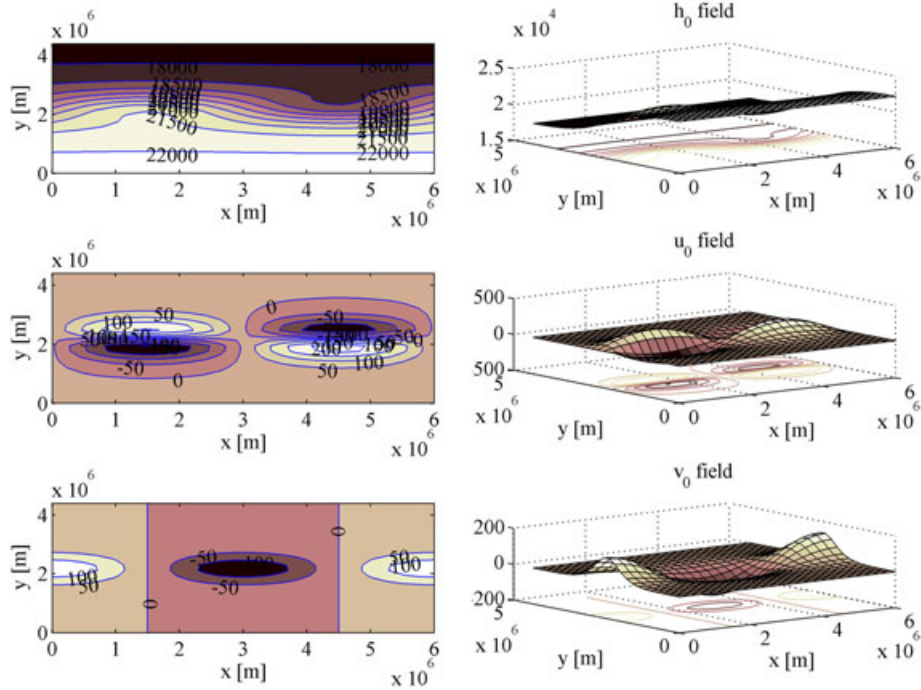
Figure 1. Geopotential height field for the Grammeltvedt initial condition h_0 and streamwise and spanwise velocity fields (u_0, v_0) calculated from the geopotential field by using the geostrophic approximation.
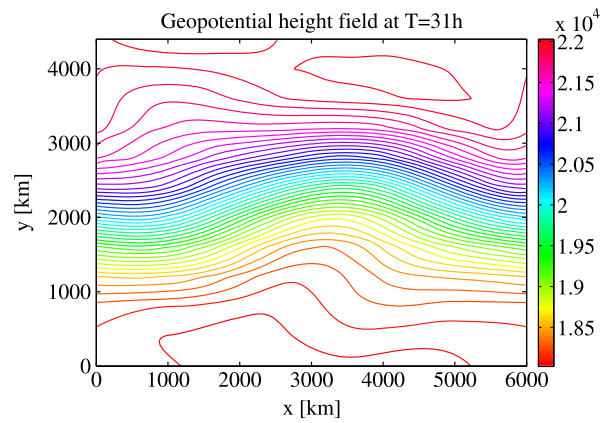

Figure 2. Solution of geopotential height field h at $T = 31h$.
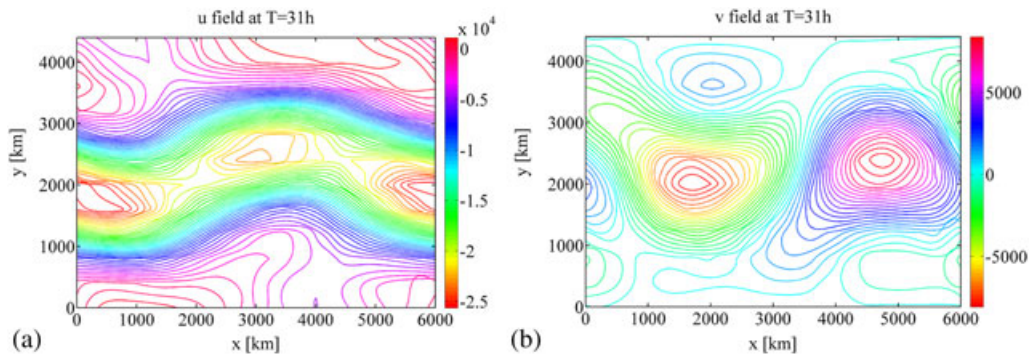

Figure 3. (a) Solution of streamwise field u and (b) solution of spanwise field v at $T = 31h$.

Table I. The number of selected modes for representation of $h, u,$ and v
fields employing criteria (9) and (11) and relative errors.

Shallow-water equations field	Selection based on amplitude criterion (9)	Selection based on dynamic criterion (11)
h	17	11
u	27	11
v	17	13
Relative error $Er_{DMD}{}^h$	3.731×10^{-4}	2.5785×10^{-4}
Relative error $Er_{DMD}{}^u$	5.8036×10^{-3}	8.6709×10^{-4}
Relative error $Er_{DMD}{}^v$	1.78×10^{-3}	1.62×10^{-3}
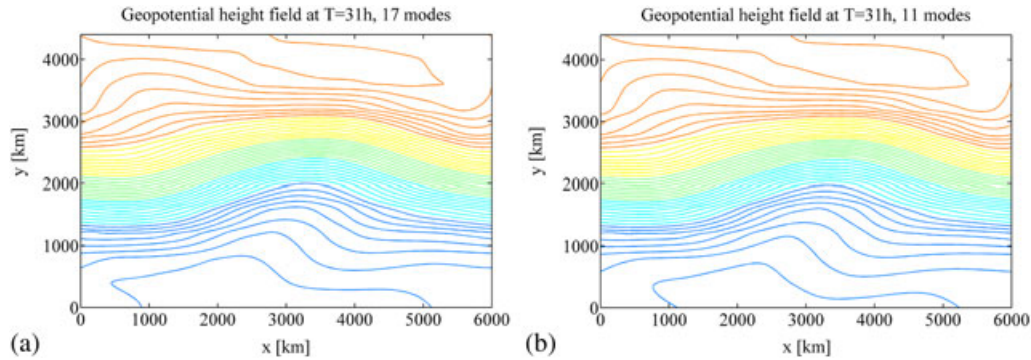
Figure 4. Reduced dynamic mode decomposition solution of geopotential height field h at $T = 31h$: (a) involving 17 dynamic modes selected with amplitude criterion (9) and (b) involving 11 dynamic modes selected with dynamic criterion (11).
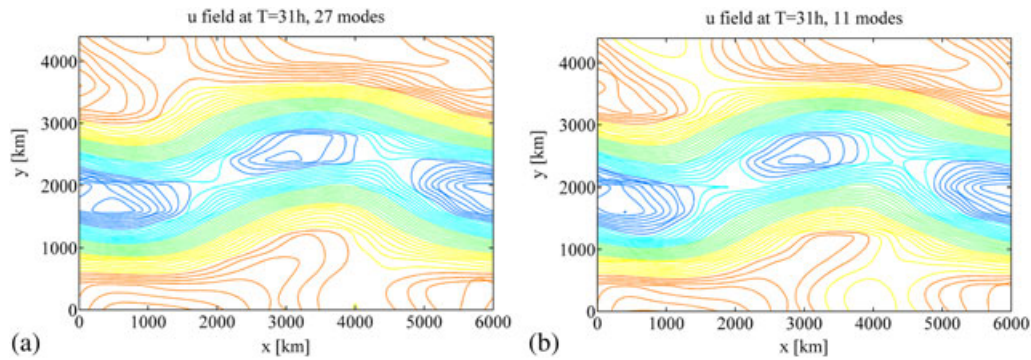
Figure 5. Reduced dynamic mode decomposition solution of u field at $T = 31h$: (a) involving 27 dynamic modes selected with amplitude criterion (9) and (b) involving 11 dynamic modes selected with dynamic criterion (11).

The selection of dynamic modes was performed employing both criteria presented herein, namely, the amplitude criterion and dynamic vector-filtering criterion. We solved the constrained optimization problems described by Eqs. (9)–(11) employing the sequential quadratic programming [54]. The number of selected modes for representation of $h, u,$ and v fields by the reduced DMD model is presented in Table I. The flow reconstructions based on the selected modes in both cases are represented respectively in Figures 4, 5, and 6 and exhibit the relative errors illustrated in Figures 7 and 8.

In case of application of the dynamic vector-filtering criterion (11) introduced in this paper, the number of dominant modes is reduced compared with the classic amplitude criterion, preserving a very good approximation of the full solution by the reduced DMD model. The benefit of the proposed filtering criterion consists in eliminating the modes that contribute weakly to the data
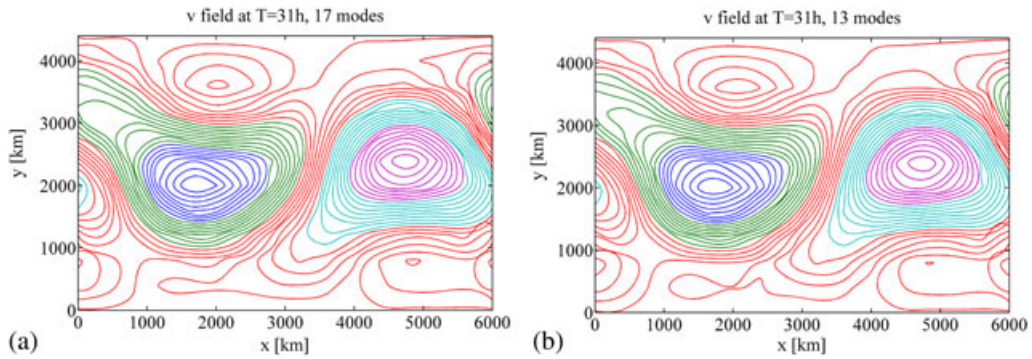
Figure 6. Reduced dynamic mode decomposition solution of v field at $T = 31h$: (a) involving 17 dynamic modes selected with amplitude criterion (9) and (b) involving 13 dynamic modes selected with dynamic criterion (11).
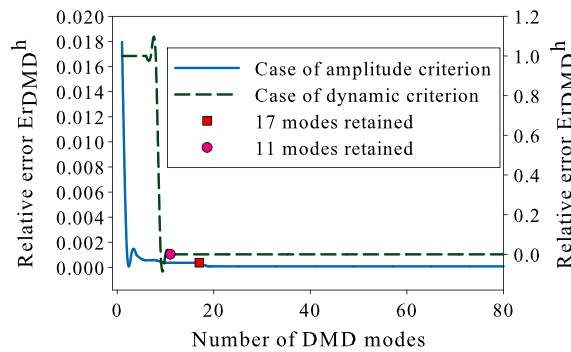

Figure 7. The relative errors computed as the retained number of dynamic modes, in case of application of the amplitude criterion (9) (17 modes) and dynamic criterion (11) (11 modes) for h field.
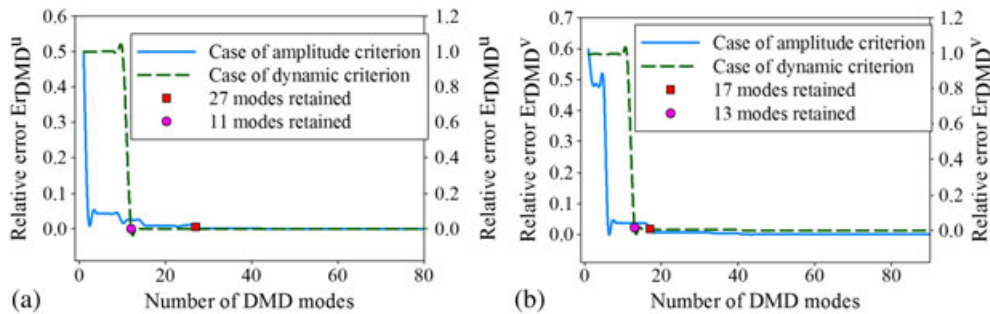

Figure 8. (a) The relative errors for u field computed as the retained number of dynamic modes, in case of application of the amplitude criterion (9) (27 modes) and dynamic criterion (11) (11 modes) and (b) the relative errors for v field, in case of application of the amplitude criterion (9) (17 modes) and dynamic criterion (11) (13 modes).

sequence. It provides an automatic selection of the most representative modes, even they exhibit rapidly growing with lower amplitudes or they are high-amplitudes fast damped modes.

The next figures illustrate the spectra of DMD. The colored Ritz values are selected by the two mentioned criteria and are associated to the selected dynamic modes involved in the reduced DMD model of the flow field. In Figures 9–14, the Ritz values selected for the reduced model of the h field, u field, and v field employing the two mentioned criteria are presented, respectively.

The figures highlight the effect of the new dynamic criterion (11) to select different modes than the classic amplitude criterion, but having the strongest impact in the reconstruction of the flow dynamics. For the shallow-water problem investigated in this section, the modes selection based on
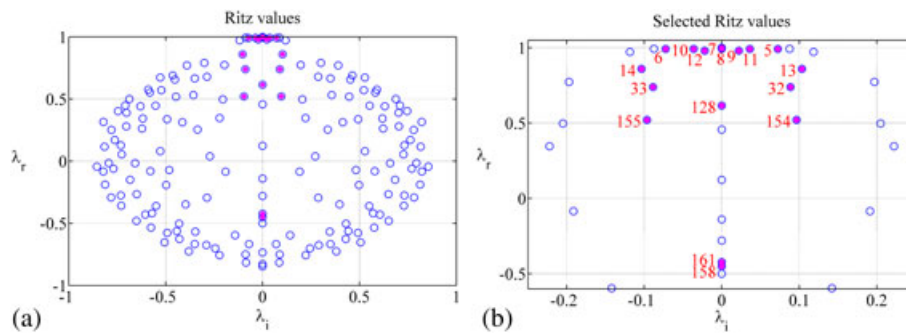
Figure 9. (a) The spectrum of dynamic mode decomposition of geopotential height field h. Colored dots represent the Ritz values with the most influential modes selected with amplitude criterion (9) (17 modes). (b) Indices of modes selected with amplitude criterion (9).
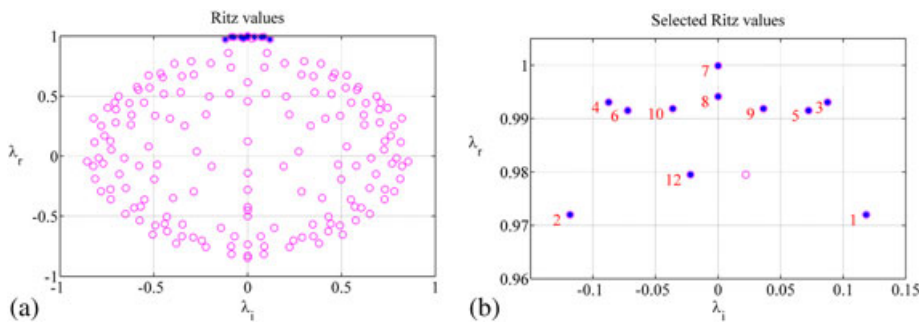
Figure 10. (a) The spectrum of dynamic mode decomposition of geopotential height field h. Colored dots represent the Ritz values with the most influential modes selected with dynamic criterion (11) (11 modes). (b) Indices of modes selected with dynamic criterion (11).
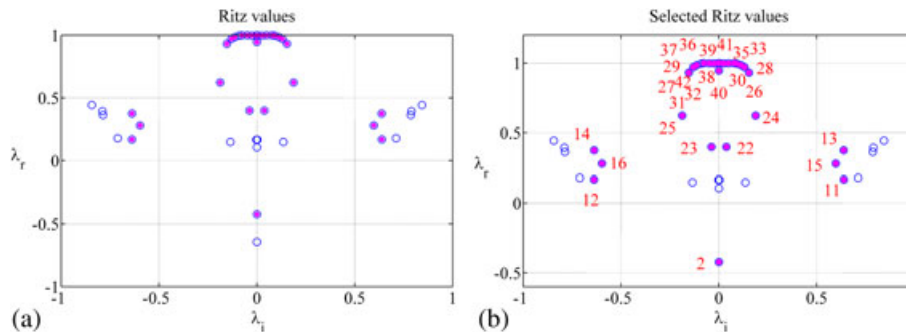
Figure 11. (a) The spectrum of dynamic mode decomposition of u field. Colored dots represent the Ritz values with the most influential modes selected with amplitude criterion (9) (27 modes). (b) Indices of modes selected with amplitude criterion (9).
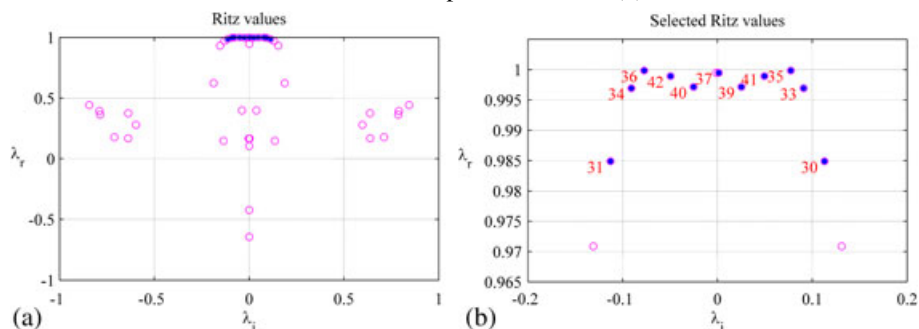
Figure 12. (a) The spectrum of dynamic mode decomposition of u field. Colored dots represent the Ritz values with the most influential modes selected with dynamic criterion (11) (11 modes). (b) Indices of modes selected with dynamic criterion (11).
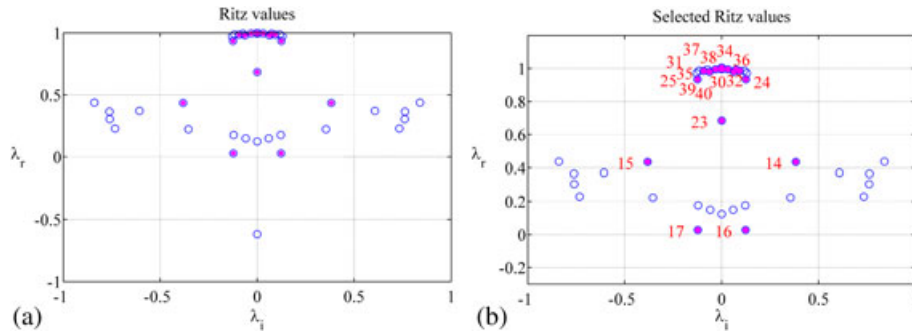
Figure 13. (a) The spectrum of dynamic mode decomposition of v field. Colored dots represent the Ritz values with the most influential modes selected with amplitude criterion (9) (17 modes). (b) Indices of selected modes selected with amplitude criterion (9).
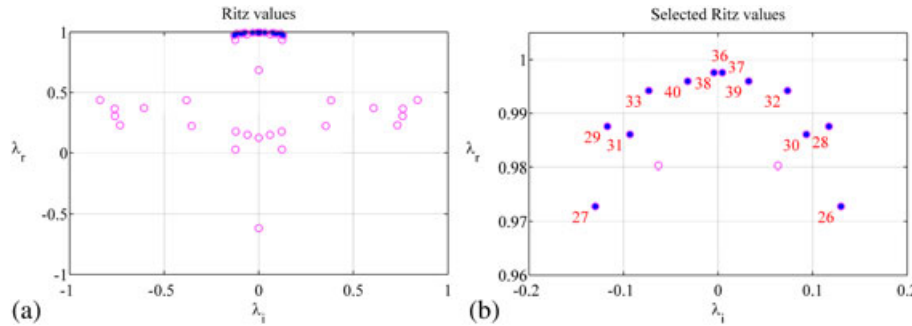

Figure 14. (a) The spectrum of dynamic mode decomposition of v field. Colored dots represent the Ritz values with the most influential modes selected with dynamic criterion (11) (13 modes). (b) Indices of modes selected with dynamic criterion (11).

the new dynamic criterion (11) proved to be more efficient than the selection based on modes amplitude. Dynamic criterion (11) is perfectly adapted to the flow dynamics and selects the significant modes for the representation of the flow model, consisting both on fast damped modes having high amplitudes and rapidly growing modes having lower amplitudes.

4. NUMERICAL RESULTS FOR SWIRLING FLOW PROBLEM

The main interest in recent decade is to use the mathematical modeling and advanced computational methods in predicting transitions between laminar and turbulent configurations for a given flow field. The challenge of this task is to build the linear dynamical system that models the evolution of the flow and to define a new mathematical and numerical methodology to compute the modes that have the strongest influence to the flow dynamics. The intent of this section is to undertake the study of a confined swirling flow dynamics, by means of DMD and to test the capabilities of the aforementioned modes selection criteria.

We consider a bounded domain $\Omega \subset \mathbb{R}^2$, and let $L^2(\Omega)$ be the Hilbert space of square integrable vector functions over Ω, associated with the energy norm $\|u\|_{L^2} = (u, u)_{L^2}^{1/2}$ and the standard inner product $(u, v)_{L^2} = \int_\Omega u \cdot v \, d\Omega$. Let H_∇ be the Hilbert space of divergence-free functions given by the following:

$$H_\nabla = \left\{ u \in L^2(\Omega) \; \middle| \; \nabla \cdot u = 0 \; in \; \Omega, \; u \cdot \vec{n} = 0 \; on \; \partial\Omega \right\}, \tag{21}$$

where $\vec{n}$ is the outward normal to the boundary. We define $H^d(\Omega) \subset L^2(\Omega)$ to be the Hilbert space of functions with d distributional derivatives that are all square integrable. Let V be the Hilbert space:

$$V = \left\{ u \in H_{\nabla} \;\middle|\; u \in H^1(\Omega), \; u = 0, \; \frac{\partial u}{\partial \vec{n}} = 0, \; on \; \partial\Omega \right\}, \tag{22}$$

with norm $\|u\|_V = (u, u)_V^{1/2}$ and the inner product $(u, v)_V = \sum\limits_{i=1}^{d} (\nabla u_i, \nabla v_i)$.

We consider the incompressible Navier–Stokes equations [55, 56] in two space dimensions, in non-dimensional form, in a rectangular domain $\Omega = [0, l_x] \times [0, l_y]$:

$$\frac{\partial u}{\partial t} = -\frac{\partial u^2}{\partial x} - \frac{\partial uv}{\partial y} - \frac{\partial p}{\partial x} + \frac{1}{Re} \left(\frac{\partial^2 u}{\partial x^2} + \frac{\partial^2 v}{\partial y^2} \right), \tag{23}$$

$$\frac{\partial v}{\partial t} = -\frac{\partial v^2}{\partial y} - \frac{\partial uv}{\partial x} - \frac{\partial p}{\partial y} + \frac{1}{Re} \left(\frac{\partial^2 u}{\partial x^2} + \frac{\partial^2 v}{\partial y^2} \right), \tag{24}$$

$$\frac{\partial u}{\partial x} + \frac{\partial v}{\partial y} = 0, \tag{25}$$

where (u, v) represents the velocity field, p is the pressure, and Re stands for the Reynolds number. Vorticity-stream function approach to two-dimensional problem of solving Navier–Stokes equations requires to remove explicitly the pressure from the Navier–Stokes equations. The vorticity for two-dimensional case is defined as follows:

$$\varsigma = |\varsigma| = \frac{\partial v}{\partial x} - \frac{\partial u}{\partial y}, \tag{26}$$

and stream function definition is as follows:

$$\frac{\partial \Psi}{\partial y} = u, \quad \frac{\partial \Psi}{\partial x} = -v. \tag{27}$$

Combining these definitions with Navier–Stokes equations (23)–(24) will eliminate pressure from the momentum equations. Non-pressure vorticity transport equation is obtained, which in non-steady form can be written as follows:

$$\frac{\partial \varsigma}{\partial t} + u \frac{\partial \varsigma}{\partial x} + v \frac{\partial \varsigma}{\partial y} = \frac{1}{Re} \left(\frac{\partial^2 \varsigma}{\partial x^2} + \frac{\partial^2 \varsigma}{\partial y^2} \right). \tag{28}$$

Having combined Eqs. (26) and (27), the Poisson equation for the stream function variable Ψ is obtained:

$$\nabla^2 \Psi = \frac{\partial^2 \Psi}{\partial x^2} + \frac{\partial^2 \Psi}{\partial y^2} = -\varsigma. \tag{29}$$

In the present numerical experiment, the vorticity-stream solution is obtained by employing the Crank–Nicolson method described by Strang in his book [57], considering no-slip boundary conditions on each wall [58] of the fixed spatial domain Ω. We have captured the swirling flow dynamics with the numerical constants $l_x = l_y = 120m$ along the integration time window $[0, 20s]$.

In order to assess the performances of the method proposed, we have considered two numerical experiments. In the first experiment, we record a number of 200 unsteady solutions of the vorticity field, with time step $\Delta t = 10^{-1}$, considering the flow in laminar regime, with Reynolds number $Re = 200$. In the second experiment, we consider the flow in turbulent regime with Reynolds number $Re = 5000$, and we decrease the time step at $\Delta t = 10^{-2}$. A number of 2000 unsteady solutions of the vorticity field have been recorded.

Figure 15(a) presents the solution of vorticity field at $T = 18s$ in laminar regime. Employing the sequential quadratic programming [54] to solve the constrained optimization problems (9) and (11), we obtain the numbers of retained modes for vorticity field, which are presented in Table II.
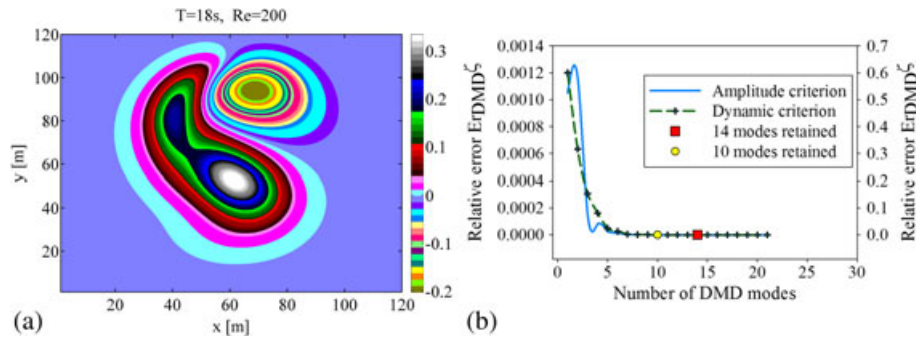
Figure 15. (a) Solution of vorticity field at $T = 18s$ in laminar regime with Reynolds number $Re = 200$ and (b) the relative errors computed as the retained number of dynamic modes, in case of application of the amplitude criterion (9) (14 modes) and dynamic criterion (11) (10 modes) for vorticity field ς.

Table II. The number of selected modes for representation of vorticity field employing criteria (9) and (11) and relative errors in laminar regime.

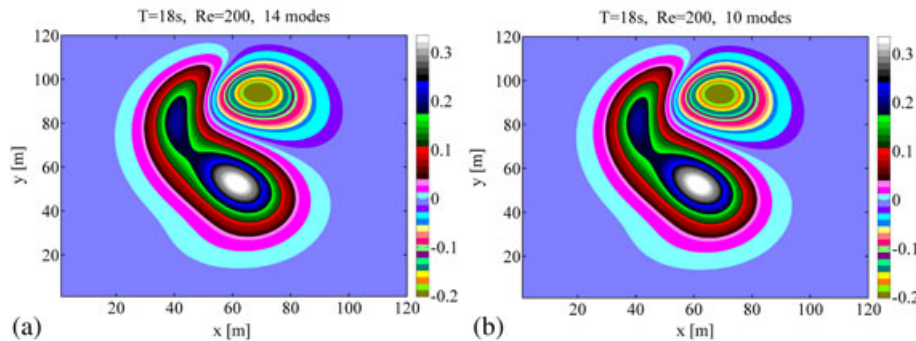| Flow regime laminar	Selection based on amplitude criterion (9)	Selection based on dynamic criterion (11)
No. of modes	14	10
Relative error $Er_{DMD}{}^{\varsigma}$	4.16×10^{-5}	4.93×10^{-5}

Figure 16. Reduced order solution of vorticity field at $T = 18s$ in laminar regime $Re = 200$, employing (a) 14 modes selected with amplitude criterion (9) and (b) 10 modes selected with dynamic criterion (11).

The amplitude criterion (9) leads to a number of 14 retained modes. The propose dynamic filtering criterion (11) selects the most influential 10 dynamic modes. The relative errors are illustrated in Figure 15(b). The vorticity field reconstruction based on the selected modes in both cases are represented, respectively, in Figure 16.

Figure 17 illustrates the spectra of DMD of vorticity field in laminar regime. The Ritz values retained for the reduced order DMD model employing both the amplitude criterion and dynamic filtering criterion introduced in this paper are marked on the figure.

Figure 18(a) presents the solution of vorticity field at $T = 18s$ in turbulent regime. The selection criteria (9) and (11) lead to the numbers of dynamic modes presented in Table III. In this experiment, the amplitude criterion (9) proved to be more efficient in terms of mode number reduction, filtering 44 influential dynamic modes, while dynamic criterion (11) selects a number of 56 dynamic modes to contribute to the reduced order model with a relative error presented in Table III and in Figure 18(b). Instead, the novel filtering technique provides a higher degree of accuracy for flow reconstruction linear model. The vorticity field reconstruction in turbulent regime based on the selected modes with both criteria is represented respectively in Figure 19.

For the problem investigated here, both criteria show satisfactory performances.
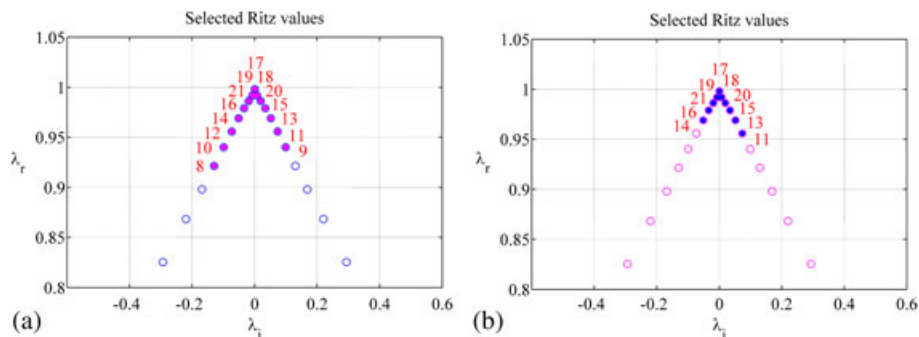
Figure 17. The spectrum of dynamic mode decomposition of vorticity field in laminar regime. Colored dots represent the Ritz values with the most influential modes selected with (a) amplitude criterion (9) (14 modes) and (b) dynamic criterion (11) (10 modes), respectively.
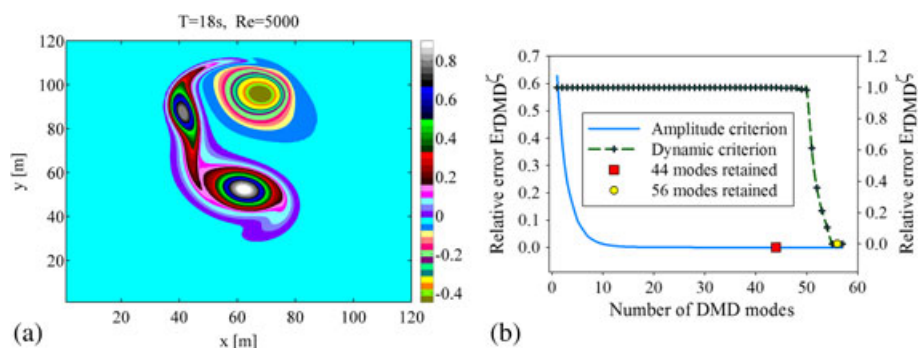

Figure 18. (a) Solution of vorticity field at $T = 18s$ in turbulent regime with Reynolds number $Re = 5000$ and (b) the relative errors computed as the retained number of dynamic modes, in case of application of the amplitude criterion (9) (44 modes) and dynamic criterion (11) (56 modes) for vorticity field ς.

Table III. The number of selected modes for representation of vorticity field employing criteria (9) and (11) and relative errors in turbulent regime.

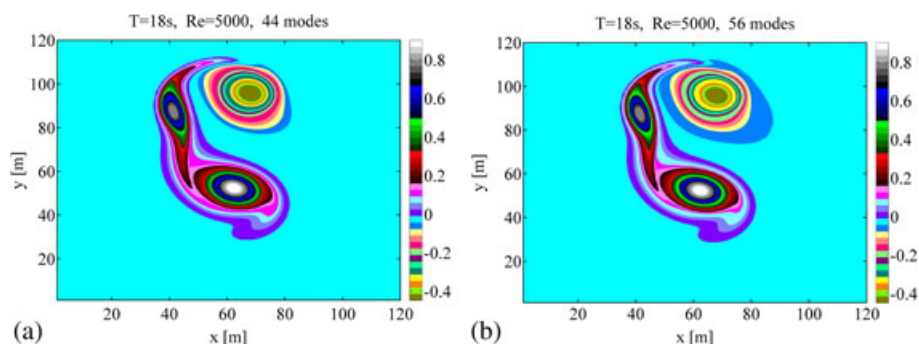| Flow regime *turbulent*	Selection based on amplitude criterion (9)	Selection based on dynamic criterion (11)
No. of modes	44	56
Relative error $Er_{DMD}{}^\varsigma$	7.57×10^{-6}	9.08×10^{-7}

Figure 19. Reduced order solution of vorticity field at $T = 18s$ in turbulent regime $Re = 5000$, employing (a) 44 modes selected with amplitude criterion (9) and (b) 56 modes selected with dynamic criterion (11).

5. SUMMARY AND CONCLUSIONS

The present investigation has focused on the effects of modes selection in dynamic modes decomposition. Based on the DMD method introduced in [21], we proposed an improved algorithm for selecting the dominant DMD modes from the flow field, and we pointed out the problems for which the new criterion proved its efficiency.

In order to assess the performances of the proposed technique, we have considered three numerical experiments, and we applied both the classic amplitude criterion and the improved selection criterion for different snapshots obtained by sampling down the original solutions of the full model. We compared the effect of the novel selection criterion with the classic one in illustrative examples originating from shallow water, laminar flows, and turbulent flows.

Unlike the classic selection based on modes amplitude, dynamic vector-filtering criterion introduced in this paper offers two major advantages: It is able to select modes with very high amplitudes but which are very fast damped, or rapidly growing modes having lower amplitudes. The new dynamic filtering criterion proved its efficiency in application to shallow-water problem and swirling flow in laminar regime. It contributes to a reduced size of the DMD model than the classic modes selection method. A different situation may occur in the case of turbulent regime. For this case, the selection of modes based on their amplitude proved to be more efficient in terms of modes number reduction, but the novel filtering technique provides a higher degree of accuracy for flow reconstruction linear model.

From the present investigation, we pointed out that the filtering of dynamic modes in DMD must be adapted to the problem that is investigated. In these benchmarks, applying the proposed filtering mode technique, the flow reconstruction error is shown to be significantly reduced.

For modeling problems with strong nonlinearities, the cost of evaluating the reduced order models still depends on the size of the full order model and therefore is still expensive. The discrete empirical interpolation method (DEIM) described in detail in [59] represents an option to further approximate the nonlinearities in the projection-based reduced order strategies. The application of a DEIM-ROM strategy combined with the DMD method proposed in this paper represents a subject that we will defer to a future study. The resulting DEIM-DMD-ROM will be evaluated efficiently at a cost that is independent of the size of the original problem.

REFERENCES

1. Luchtenburg DM, Rowley CW. Model reduction using snapshot-based realizations. *64th Annual Meeting of the APS Division of Fluid Dynamics American Physical Society*, Baltimore, 2011; H19.004.
2. Liberge E, Hamdouni A. Reduced order modelling method via proper orthogonal decomposition (POD) for flow around an oscillating cylinder. *Journal of Fluids and Structures* 2010; **26**:292–311.
3. Wang Z, Akhtar I, Borggaard J, Iliescu T. Proper orthogonal decomposition closure models for turbulent flows: a numerical comparison. *Computer Methods in Applied Mechanics and Engineering* 2012; **237-240**:10–26.
4. Abramov RV, Majda AJ. Low-frequency climate response of quasigeostrophic wind-driven ocean circulation. *Journal of Physical Oceanography* 2012; **42**:243–260.
5. Dumon A, Allery C, Ammar A. Proper generalized decomposition method for incompressible Navier–Stokes equations with a spectral discretization. *Applied Mathematics and Computation* 2013; **219**(15):8145–8162.
6. Osth J, Noack BR, Krajnovic S, Barros D, Boree J. On the need for a nonlinear subscale turbulence term in POD models as exemplified for a high-Reynolds-number flow over an Ahmed body. *Journal of Fluid Mechanics* 2014; **747**:518–544.
7. Mariani R, Dessi D. Analysis of the global bending modes of a floating structure using the proper orthogonal decomposition. *Journal of Fluids and Structures* 2012; **28**:115–134.

8. Buljak V, Maier G. Proper orthogonal decomposition and radial basis functions in material characterization based on instrumented indentation. *Engineering Structures* 2011; **33**:492–501.

9. Xiao M, Breitkopf P, Coelho RF, Knopf-Lenoir C, Villon P, Zhang W. Constrained proper orthogonal decomposition based on QR-factorization for aerodynamical shape optimization. *Applied Mathematics and Computation* 2013; **223**:254–263.

10. Du J, Fang F, Pain CC, Navon IM, Zhu J, Ham D. POD reduced order unstructured mesh modelling applied to 2d and 3d fluid flow. *Computers and Mathematics with Applications* 2013; **65**:362–379.

11. Fang F, Pain CC, Navon IM, Piggott MD, Gorman GJ, Allison P, Goddard AJH. Reduced order modelling of an adaptive mesh ocean model. *International Journal for Numerical Methods in Fluids* 2009; **59**(8):827–851.

12. Stefanescu R, Sandu A, Navon IM. Comparison of POD reduced order strategies for the nonlinear 2d shallow water equations. *International Journal for Numerical Methods in Fluids* 2014; **76**(8):497–521.

13. Dimitriu G, Navon IM, Stefanescu R. Application of POD-DEIM approach for dimension reduction of a diffusive predator-prey system with Allee effect. *Large-Scale Scientific Computing* 2014; **8353**:373–381.

14. Xiao D, Fang F, Pain C, Hu G. Non-intrusive reduced-order modelling of the Navier-Stokes equations based on RBF interpolation. *International Journal for Numerical Methods in Fluids* 2015; **79**(11):580–595.

15. Winton C, Pettway J, Kelley CT, Howington S, Eslinger OJ. Application of proper orthogonal decomposition (POD) to inverse problems in saturated groundwater flow. *Advances in Water Resources* 2011; **34**:1519–1526.

16. Chen X, Navon IM, Fang F. A dual-weighted trust-region adaptive POD 4D-VAR applied to a finite-element shallow-water equations model. *International Journal for Numerical Methods in Fluids* 2011; **65**:250–541.

17. Chen X, Akella S, Navon IM. A dual-weighted trust-region adaptive POD 4-D VAR applied to a finite-volume shallow water equations model on the sphere. *International Journal for Numerical Methods in Fluids* 2012; **68**: 377–402.

18. Cao Y, Zhu J, Luo Z, Navon IM. Reduced order modeling of the upper tropical Pacific ocean model using proper orthogonal decomposition. *Computers and Mathematics with Applications* 2006; **52**(8-9):1373–1386.

19. Cao Y, Zhu J, Navon IM, Luo Z. A reduced order approach to four-dimensional variational data assimilation using proper orthogonal decomposition. *International Journal for Numerical Methods in Fluids* 2007; **53**(10):1571–1583.

20. Chen KK, Tu JH, Rowley CW. Variants of dynamic mode decomposition: boundary condition, Koopman and Fourier analyses. *Nonlinear Science* 2012; **22**:887–915.

21. Rowley CW, Mezic I, Bagheri S, Schlatter P, Henningson DS. Spectral analysis of nonlinear flows. *Journal of Fluid Mechanics* 2009; **641**:115–127.

22. Schmid PJ. Dynamic mode decomposition of numerical and experimental data. *Journal of Fluid Mechanics* 2010; **656**:5–28.

23. Schmid PJ, Violato D, Scarano F. Decomposition of Time-resolved Tomographic PIV. *Experiments in Fluids* 2012; **52**(6):1567–1579.

24. Schmid PJ, Sesterhenn J. Dynamic mode decomposition of numerical and experimental data. *61st Annual Meeting of the APS Division of Fluid Dynamics*, San Antonio, Texas, Vol. 53, No. 15, 2008.

25. Koopman B. Hamiltonian systems and transformations in Hilbert space. *Proceedings of the National Academy of Sciences* 1931; **17**:315–318.

26. Fiedler M. A note on companion matrices. *Linear Algebra and its Applications* 2003; **372**:325–331.

27. Rowley CW, Mezic I, Bagheri S, Schlatter P, Henningson DS. Reduced-order models for flow control: balanced models and Koopman modes. In *Proceedings of the Seventh IUTAM Symposium on Laminar-Turbulent Transition*: Stockholm, Sweden, 2009; 43–50.

28. Muld TW, Efraimsson G, Henningson DS. Flow structures around a high-speed train extracted using proper orthogonal decomposition and dynamic mode decomposition. *Computers and Fluids* 2012; **57**:87–97.

29. Schmid PJ, Meyer KE, Pust O. Dynamic mode decomposition and proper orthogonal decomposition of flow in a lid-driven cylindrical cavity. *8th International Symposium on Particle Image Velocimetry - PIV09*, Melbourne, 2009, Article in proceedings.

30. Frederich O, Luchtenburg DM. Modal analysis of complex turbulent flow. *The 7th International Symposium on Turbulence and Shear Flow Phenomena (TSFP-7)*, Ottawa, Canada, 2011.

31. Balajewicz MJ, Dowell EH, Noack BR. Low-dimensional modelling of high-Reynolds-number shear flows incorporating constraints from the Navier–Stokes equation. *Journal of Fluid Mechanics* 2013; **729**:285–308.

32. Mezic I. Spectral properties of dynamical systems, model reduction and decompositions. *Nonlinear Dynamics* 2005; **41**(1-3):309–325.

33. Mezic I. Analysis of fluid flows via spectral properties of the Koopman operator. *Annual Review of Fluid Mechanics* 2013; **45**(1):357–378.

34. Noack BR, Stankiewicz W, Morzynski M, Schmid PJ. Recursive dynamic mode decomposition of a transient cylinder wake. *physics.flu-dyn arXiv:1511.06876v1* 2015.

35. Bistrian DA, Navon IM. An improved algorithm for the shallow water equations model reduction: dynamic mode decomposition vs POD. *International Journal for Numerical Methods in Fluids* 2014; **78**(9):552–580.

36. Jovanovic MR, Schmid PJ, Nichols JW. Low-rank and sparse dynamic mode decomposition. *Center for Turbulence Research Annual Research Briefs* 2012:139–152.

37. Bagheri S. Koopman-mode decomposition of the cylinder wake. *Journal of Fluid Mechanics* 2013; **726**:596–623.

38. Belson B, Tu JH, Rowley CW. Algorithm 945: modred – a parallelized model reduction library. *ACM Transactions on Mathematical Software* 2014; **40**(4):Article No. 30:1–30.

39. Williams MO, Kevrekidis IG, Rowley CW. A data driven approximation of the Koopman operator: extending dynamic mode decomposition. *Nonlinear Science* 2015; **25**(6):1307–1346.
40. Chopra AK. *Dynamics of Structures* (4th edn). Prentice-Hall International Series in Civil Engineering and Engineering Mechanics, 2000.
41. Tissot G, Cordier L, Benard N, Noack BR. Model reduction using dynamic mode decomposition. *Comptes Rendus Mecanique* 2014; **342**:410–416.
42. Noak BR, Morzynski M, Tadmor G. *Reduced-order Modelling for Flow Control*. Springer-Verlag Wien, 2011.
43. Nyquist H. Certain topics in telegraph transmission theory. *Transactions of the American Institute of Electrical Engineers* 1928; **47**(2):617–644.
44. Bryden IG, Couch SJ, Owen A, Melville G. Tidequations resource assessment. *Proceedings of the IMechE, Part A: Journal of Power and Energy* 2007; **221**:125–135.
45. Sportisse B, Djouad R. Reduction of chemical kinetics in air pollution modeling. *Journal of Computational Physics* 2000; **164**:354–376.
46. Koutitus C. *Mathematics Models in Coastal Engineering*. Pentech Press: London, 1988.
47. Vreugdenhil CB. *Numerical Methods for Shallow Water Flow*. Kluwer Academic Publishers: Dordrecht; Boston, 1994.
48. Navon IM. FEUDX: a two-stage, high accuracy, finite-element Fortran program for solving shallow-water equations. *Computers and Geosciences* 1987; **13**(3):255–285.
49. Grammeltvedt A. A survey of finite-difference schemes for the primitive equations for a barotropic fluid. *Monthly Weather Review* 1969; **97**(5):384–404.
50. Cullen MJP, Morton KW. Analysis of evolutionary error in finite-element and other methods. *Journal of Computational Physics* 1980; **34**:245–267.
51. Navon IM. Finite-element simulation of the shallow-water equations model on a limited area domain. *Applied Mathematical Modeling* 1979; **3**:337–348.
52. Stefanescu R, Navon IM. POD/DEIM nonlinear model order reduction of an ADI implicit shallow water equations model. *Journal of Computational Physics* 2013; **237**:95–114.
53. Fang F, Pain CC, Navon IM, Cacuci DG, Chen X. The independent set perturbation method for efficient computation of sensitivities with applications to data assimilation and a finite element shallow water model. *Computers and Fluids* 2013; **76**:33–49.
54. Nocedal J, Wright SJ. *Numerical Optimization* (2nd edn). Springer-Verlag: New York, 2006.
55. Galdi G. *An Introduction to the Mathematical Theory of the Navier–Stokes Equation*. Springer-Verlag: New York, 1994.
56. Davis L, Pahlevani F. Semi-implicit schemes for transient Navier–Stokes equations and eddy viscosity models. *International Journal of Numerical Methods for Partial Differential Equations* 2009; **25**:212–231.
57. Strang G. *Computational Science and Engineering*. Massachusetts Institute of Technology. Wellesley-Cambridge Press, 2007.
58. Foreman MGG. On no-slip boundary conditions for the incompressible Navier–Stokes equations. *Dynamics of Atmospheres and Oceans* 1988; **12**(1):47–70.
59. Antil H, Heinkenschloss M, Sorensen D. In *Reduced Order Methods for Modeling and Computational Reduction*, chap. Application of the Discrete Empirical Interpolation Method to Reduced Order Modeling of Nonlinear and Parametric Systems. Springer, 2014; 101–136.